Original Article

Institution of MECHANICAL ENGINEERS

Journal of MATERIALS: DESIGN AND APPLICATIONS

Proc IMechE Part L:
J Materials: Design and Applications
0(0) 1–9

DOI: 10.1177/1464420715612827
pil.sagepub.com

SAGE

Influence of aramid fibers on the mechanical behavior of a hybrid carbon–aramid–reinforced epoxy composite

Gonzalo Pincheira[1], Cristian Canales[2], Carlos Medina[1], Eduardo Fernández[3] and Paulo Flores[3]

Abstract

This article is focused on the study of the contribution of aramid fibers in a hybrid carbon–aramid fiber twill weave used to reinforce epoxy resin. To evaluate the influence of the aramid fibers, a comparative study between carbon and carbon–aramid woven–reinforced composites, considering the mechanical behavior of both materials under several loading conditions, is performed. The tests used in this study are meant to analyze the effect of aramid reinforcements on the composite stiffness, strength, impact, and fracture performance. Higher values of energy absorption and fracture toughness were exhibited by the carbon–aramid composite. The mechanical tests performed indicated that the aramid phase present in the hybrid carbon–aramid composite induced an important enhancement on the impact (37.9% in energy absorption) and fracture resistance (12.7% for fracture initiation and 43% for steady state regime), compared to small reductions on the material stiffness. In addition, the ultimate strain and the through thickness compression strength were favorably affected, with an increase up to 19.5% and 8.3%, respectively, by the presence of aramid fiber that presents a more ductile response with respect to the carbon reinforcement.

Keywords

Aramid reinforcement, carbon reinforcement, hybrid composite, impact resistance, fracture toughness, carbon–aramid reinforcement

Date received: 28 August 2015; accepted: 28 September 2015

Introduction

In the last decades, an increasing demand for hybrid composites has arisen in a wide variety of fields. Properties such as high stiffness and strength, light weight, and adaptability are the main reason to select this type of materials, especially in aeronautical and automotive applications (see e.g., Friedrich and Almajid[1] and Foster[2]). The market offers a wide variety of materials and formats to develop tailor-made composite materials. Designers must be aware of the influence of the selected materials over the required properties. However, technical data sheets only contain limited information, so designers must perform experimental or numerical campaigns to compile the needed data for optimal designing. In general, the enhancement of some mechanical properties by replacement of materials might induce a reduction of other properties, which must be quantified to facilitate designing decisions (see e.g., Kretsis,[3] Ashby and Bréchet,[4] Ashby,[5] and Nunna et al.[6]).

Carbon–fiber–reinforced epoxy composites are widely used due to the competitive stiffness (and strength) to weight ratio with respect to other structural materials as discussed by Gay and Hoa[7] and Nicolais et al.[8] Carbon fibers can be selected to achieve high strength or high modulus, but present low elongation (see e.g., Rahmani et al.[9]). Thus, it is possible to incorporate another reinforcement into the composite in order to compensate the carbon fiber fragility. A material that normally appears as a

[1]Department of Materials Engineering, University of Concepción, Concepción, Chile
[2]Department of Aerospace & Mechanical Engineering, University of Liège, Liège, Belgium
[3]Department of Mechanical Engineering, University of Concepción, Concepción, Chile

Corresponding author:
Paulo Flores, Department of Mechanical Engineering, University of Concepción, Edmundo Larenas 270 Interior, Concepción 4030000, Chile.
Email: pfloresv@udec.cl

suitable alternative in this case is the aramid fiber. Compared to the mechanical properties of high strength carbon fiber, the aramid fibers have a lower density, stiffness, and strength, but present higher elongation and fracture toughness as can be seen in CES.[10]

Since the early work of Hayashi[11] and Phillips,[12] the behavior of hybrid composite materials has been studied by several authors under different mechanical conditions both experimentally and numerically. Zweben[13] presented a statistical approach to determine the tensile behavior of hybrid composite by considering two simple idealized models with different failure mechanism. Fariborz et al.[14] introduced a probabilistic model to estimate the behavior of intraply hybrids under tensile conditions. More recently, Pandya et al.[15] reported an experimental analysis of the tensile properties of hybrid composites considering glass and carbon laminates with epoxy resin; the results shown that the stacking sequence played an important role for the tensile strength and ultimate strain after hybridization. This finding was later corroborated by the work of Zhang et al.[16] and Banerjee and Sankar[17] by means of further experiments and numerical simulations, respectively. Li et al.[18] presented experimental results that shown a positive hybrid effect in the compressive strength, flexural modulus, and flexural strength. Dong and Davies[19,20] simulated the behavior of unidirectional glass–carbon/epoxy composites in order to find the optimal hybrid flexural response; the strength was significantly improved by the hybridization when compared with those of full carbon or glass composites. Hosur et al.[21] analyzed the mechanical behavior of hybrid composites plates under low-velocity impact loading. Valença et al.[22] performed tensile, bending, and impact tests in order to examine the hybrid behavior of glass–kevlar/epoxy composites; greater values of specific tensile strength, bending stiffness, and strength as well as energy absorption were exhibited by the hybrid composites.

Some efforts have been also made to investigate the effect of hybridization considering carbon and aramid fibers as reinforcement of epoxy resin. Chiu[23] performed compression and impact tests to study the failure modes of carbon and hybrid carbon–aramid composites tubes; the results indicated improved crashworthiness behavior and also indicated a small decrease in the amounts of the absorbed energy for carbon–aramid tubes. Kostar et al.[24] reported an increase of the tensile modulus and the ultimate strength for carbon–aramid hybrid weaves with respect to carbon/epoxy composites. Wan et al.[25] studied the influence of the Kevlar fiber volume fraction in carbon–Kevlar/epoxy hybrid materials; positive effects were found for the flexural properties and the impact strength with increasing Kevlar content. The mechanical properties computed by Song[26] from tensile and bending experiments shown that the presence of carbon fibers completely dominated the response of the hybrid composites. Dorey et al.[27] and Marom et al.[28] analyzed the impact behavior of carbon–kevlar hybrid composites with different stacking configurations; in both studies, it was noticed a significant positive hybrid effect with a strong dependency on the stacking sequence. Ma et al.[29] studied the energy absorption capacity of carbon and carbon–aramid fiber–reinforced composite tubes under quasi-static conditions. It was found that carbon–aramid hybrid composites presented a better capacity to absorb energy than carbon composite tubes. It is worth to mention that a great part of these studies were performed considering multilayered hybridization of full carbon and aramid plies for particular applications.

In this work, we concentrated on the study of aramid–fiber contribution found in hybrid carbon–aramid twill weaves used as reinforcement for epoxy resin. To evaluate the influence of the aramid fibers, we studied the mechanical behavior of the hybrid carbon–aramid composite under several loading conditions, and then, we compared the results to those obtained using a carbon fiber woven reinforcement with similar characteristics. We focused the tests to evaluate the influence of aramid fibers on the composite stiffness and strength (tensile, out-of-plane compression, and in-plane shear), impact performance, and fracture behavior. These results are greatly useful in the design composite materials for high-performance applications, but they are not easily found in the literature and rarely gathered in a single report.

Materials and manufacturing

Selected materials

The matrix is composed of the L20 epoxy resin with an EPH 161 hardener, which is produced by Momentive, USA and was purchased from R&G composites, Germany. According to the technical data from the manufacturer, this resin system is designed for heat resistant components up to 120 °C and groutings of up to approximately 10 mm thick. In addition, curing occurs virtually free of shrinkage. The resin viscosity in solution with the hardener at 25 °C is 700 cP and at 35 °C is 295 cP (the measurements were performed using a Fungilab Alpha series rotational viscometer).

The reinforcements are: (1) a carbon twill woven fabric of 204 g/m^2 and (2) a hybrid carbon (61%) aramid (39%) twill woven fabric of 210 g/m^2, with the same distribution (61% carbon—39% aramid) in both warp and weft directions. The carbon fibers are Tenax® E HTA40 3 K and the aramid fibers are Twaron® 2200. The fabrics are manufactured by Engineered Cramer Composites, Germany.

Manufacturing process

The materials were manufactured by RTM. In this procedure, the resin was injected into the mold at 4 bar, and then the composite was cured at room temperature for 24 h and then post-cured for 15 h at 100 °C. The mixing ratio of the composite was 100:25 parts by weight of resin to hardener, which was mixed via mechanical stirring at room temperature.

Two composites geometries were manufactured for both materials, carbon/epoxy fiber (CF/EP) and carbon–aramid/epoxy fiber (CAF/EP), by means of the procedure described above. The first one was a 12-ply laminate of 544 mm × 250 mm × 2.8 mm that was used to characterize the in-plane mechanical behavior. The second one was a 45-ply laminate of 250 mm × 150 mm × 10 mm that was used to obtain the specimens for the through thickness compression, in-plane mode I fracture toughness analysis, and tribological tests. For the two geometrical configurations, a layup angle of 0° was considered.

Laminates features

The laminate thickness was measured at a minimum of 10 points per manufactured laminate using a vernier caliper. The density was measured by the immersion method according to the ASTM D 792 standard (five samples per material). The fiber volume fraction V_f was computed according to the ASTM D 3171 (method II) standard, as follows

$$V_f = \frac{N \times \rho_{pf}}{t \times \rho_f} \quad (1)$$

where N is the number of plies in the composite, ρ_{pf} is the planar density of the fabric, t is the thickness of the laminate, and ρ_f corresponds to the density of the fibers.

The hardness was measured using a Barcol (Impressor GYZJ-934-1) according to the ASTM D 2583 standard, and the micro-Vickers hardness (using 500 g load during 10 s) was also measured for the 45-ply laminates. The above-described information is collected in Table 1.

Table 1. Laminate features.

Number of plies	Material	Parameter	AV	SD	RSD
12	CF/EP	Thickness (mm)	2.81	0.08	2.8
		Density (g/cm^3)	1.46	0.01	0.7
		Fiber volume fraction	0.49	0.02	4.1
		Barcol hardness	65.1	4.7	7.2
	CAF/EP	Thickness (mm)	2.82	0.08	2.8
		Density (g/cm^3)	1.41	0.02	1.5
		Fiber volume fraction	0.55	0.02	4.2
		Barcol hardness	58.9	6.5	11.0
45	CF/EP	Thickness (mm)	10.18	0.04	0.4
		Density (g/cm^3)	1.45	0.01	0.7
		Fiber volume fraction	0.52	0.01	1.9
		Barcol hardness	61.7	3.6	5.8
		Micro-Vickers hardness	38.0	14.0	37.0
	CAF/EP	Thickness (mm)	10.10	1.0	9.9
		Density (g/cm^3)	1.42	0.01	0.7
		Fiber volume fraction	0.57	0.02	3.9
		Barcol hardness	56.2	5.6	10.0
		Micro-Vickers hardness	32.9	10.6	32.2

Note: AV: average value; *SD*: standard deviation; RSD: relative standard deviation; CF/EP: carbon/epoxy fiber; CAF/EP: carbon–aramid/epoxy fiber.

Mechanical testing

Tensile tests

The tensile tests were performed according to the ASTM D 3039 standard, using a crosshead speed of 1 mm/min. The specimens were obtained from the 12-ply laminates. The specimens were clamped using hydraulic wedge grips. The stress was computed from the load cell data and the initial specimen cross section. The longitudinal strain was measured by means of a strain gage (length: 9.5 mm, width: 3.5 mm, gage length: 5 mm, gage factor 2.1, gage resistance: 120 Ω). The elastic modulus was computed by linear regression on the linear (elastic) range of the stress strain curve, and the tensile strength was set at the maximal stress level.

In-plane shear tests

The in-plane shear tests were performed according to the ASTM D 4255 standard, using a crosshead speed of 0.3 mm/min. A two-rails testing device is embedded in the testing machine. Specimens were obtained from the 12-ply laminates. The stress was computed from the load cell data and the initial specimen cross section. The shear strain was measured by means of a strain gage (length: 9.5 mm, width: 3.5 mm, gage length: 5 mm, gage factor 2.1, gage resistance: 120 Ω) placed as indicated in the standard. The in-plane shear modulus was obtained using a linear approach for a shear strain range of 0–0.002 (due to the nonlinear elastic–plastic behavior of the material under the imposed condition) and the shear strength was set at the achievement of a shear strain of 0.05, according to the standard.

Out-of-plane compression test

The out-of-plane compression tests were performed according to Kim et al.[30] at a crosshead speed of 0.5 mm/min. The specimens were 10 mm × 10 mm × 10 mm cubes obtained from the 45-ply laminates. The specimens were compressed between two lubricated steel plates. The stress was computed from the load cell data and the initial specimen cross section.

The longitudinal strain was measured using a strain gage (length: 6 mm, width: 2.5 mm, gage length: 2 mm, gage factor 2.0, gage resistance: 120 Ω). The through-thickness compressive elastic modulus was computed using a linear regression on the linear (elastic) range of the stress–strain curve and the through-thickness compression strength was set at the maximal stress level.

Charpy test

The Charpy test was performed over un-notched specimens (10 mm × 10 mm × 57 mm). The span to width ratio of each specimen was 5. The pendulum hammer had a mass of 20 kg, with an arm length of 770 mm; the impact speed was 5.42 m/s and the stored energy was 293.8 J. The amount of energy absorbed by the material during fracture due to the impact is recorded.

Fracture toughness (Mode I)

Several attempts have been made to predict fracture in laminated composite materials considering all of the mechanisms involved in the failure process. Some models consider the experimental results of crack growth resistance curves (R-curve) to take into account the effect fiber tensile fracture. Thus, a high accuracy in the experimental determination of the R-curve is required.

A novel procedure to determine the crack resistance curves was recently proposed by Catalanotti et al.,[31] where the computation of the J-integral is based on the displacement and the strain fields obtained by a Digital Image Correlation (DIC) system (this method appears to be able to handle some of the issues shown by previous attempts as mentioned by Pinho et al.[32]).

The crack length measurement procedure and the J-integral computation algorithm presented by Catalanotti et al.[31] were implemented (in a Matlab script) to obtain the associated R-curves on compact tension (CT) tests.

The geometry of the CT specimens is based on the ASTM E399 standard considering $w = 41$ mm. The laminated composites plates were cut to their final shape using a water-jet cutting machine. The CT specimens were painted with white and black ink to create the random pattern required by the DIC system (Aramis 5 M Lt, from GOM Gmbh).

The area considered to the displacement measurements and the strain computation was set to 25×25 mm^2. The facet size and the facet step were both fixed to 15×15 pixels, to ensure a good agreement between precision and spatial resolution on the computed data.

Four CT tests were performed for each material, recording both the displacement driven by the servo-hydraulic testing system and the applied load (measured by the embedded load cell) data. The full experimental setup of CT tests can be seen in Figure 1.

Results and discussion

Mechanical properties

The obtained mechanical properties for CF/EP and CAF/EP composites from quasi-static tensile, shear, and compression tests are summarized in Table 2. A summary of the response and material properties of both composites is shown in Figure 2. In Figure 2(a), the stress–strain curves resulting from different tests considered for the mechanical characterization are presented. The normalized material parameters of the CAF/EP composite with respect to the values from the CF/EP composite are shown in Figure 2(b), in order to facilitate the comparison of the mechanical features under consideration.

As can be seen in Figure 2(b), a reduction of 10.4% and 11.7% was observed on the hybrid CAF/EP material elastic modulus and tensile strength, respectively. In addition, the ultimate strain suffers an important increase of 8.3%. This behavior is due to the presence of the aramid phase on the CAF/EP laminates, which presents a less stiffer yet more ductile response under uniaxial tensile conditions compared to carbon fiber (see e.g., Ashby[5] and Campbell[33]). The enhancement of the measured ultimate strain is in agreement with the previous work of Manders and Bader[34] and Pandya et al.[15] Manders and Bader partially attributed this phenomenon to internal compressive strains induced during cooling in the cure step due to differential thermal contraction of the constituents.

Both the shear modulus and the shear values were reduced by 15.2% and 4.1%, respectively. This reduction comes from the superior response on in-plane shear of carbon reinforcements (CF/EP) against the aramid (CAF/EP) as discussed by Campbell.[33]

The through-thickness compression modulus presented a reduction of 24.1%, while the through-thickness compression strength shown an increase of 19.5%. It can be established that the weaker behavior of aramid fiber negatively affected the out-plane compression stiffness of the composite. Nevertheless, the aramid reinforcement seems to enhance the out-plane compression strength of the material.

Figure 3 shows the clear differences on failure patterns between CF/EP and CAF/EP materials. It is possible to see that shear appears as the main mode of failure in the CF/EP specimen (Figure 3(a)) in good agreement with previous experimental observations made by Kim et al.[30] and numerical findings presented by González and Llorca,[35] while in the CAF/EP specimen, both shear and delamination failure modes are present (Figure 3(b)). This difference can be attributed to a greater ductility of the aramid fibers

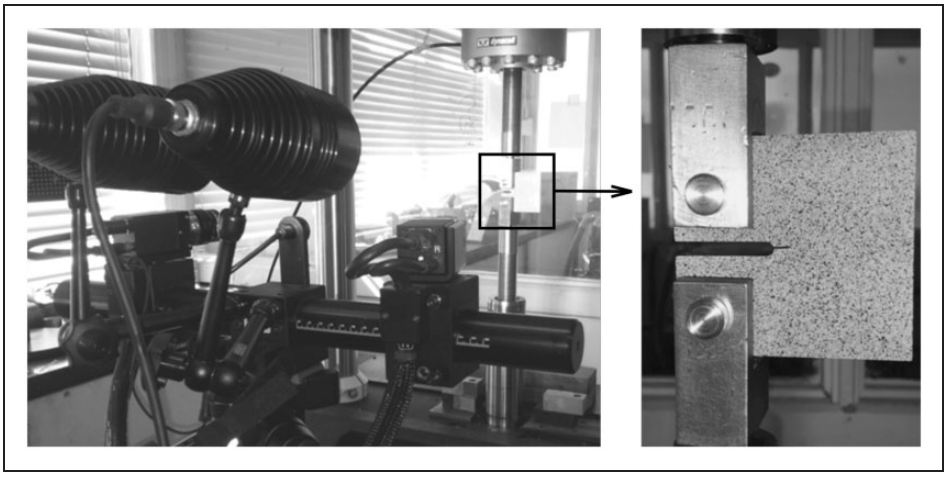

Figure 1. Experimental setup of the DIC system and compact tension specimen.

Table 2. Mechanical properties.

Test	Parameter	Material	AV	SD	RSD	CI (95%)
Tensile	Elastic modulus (GPa)	CF/EP	54.1	1.4	2.6	±1.7
		CAF/EP	48.5	2.2	4.5	±2.7
	Tensile strength (MPa)	CF/EP	692	81	11.7	±100
		CAF/EP	611	39	6.4	±48
	Poisson coefficient	CF/EP	0.058	0.008	13.8	±0.001
		CAF/EP	0.053	0.001	1.9	±0.001
	Ultimate strain	CF/EP	0.012	0.001	8.3	±0.001
		CAF/EP	0.013	0.001	7.7	±0.001
In-plane shear	Shear modulus (GPa)	CF/EP	3.3	0.6	18.2	±1.0
		CAF/EP	2.8	0.1	3.6	±0.2
	Shear strength (MPa)	CF/EP	49	3.4	6.9	±5.5
		CAF/EP	47	0.6	1.3	±1.0
Trough thickness compression	Elastic modulus (GPa)	CF/EP	8.7	0.8	9.2	±1.0
		CAF/EP	6.6	1.4	21.2	±1.7
	Compressive strength (MPa)	CF/EP	637	20	3.1	±25
		CAF/EP	761	12	1.6	±15

Note: AV: average value; *SD*: standard deviation; RSD: relative standard deviation; CI: confidence interval; CF/EP: carbon/epoxy fiber; CAF/EP: carbon–aramid/epoxy fiber.

in the CAF/EP specimens in comparison with carbon fibers, which favored the interlaminar failure and involved a higher level of compressive strength. By the contrary, a lower level of energy is required to propagate cracks in the CF/EP specimens due to a more brittle behavior of the carbon fibers.

Fracture properties

The resulting absorbed energy and fracture toughness parameters from Charpy and CT tests are presented in Table 3. For the sake of simplicity, a comparative diagram with normalized values of the CAF/EP composite with respect to CF/EP material is shown in Figure 4. The CAF/EP composite presented a superior response on both experiments.

The CAF/EP laminates presented a tougher response with respect to the CF/EP laminates, an increase of 37.9% for the absorbed energy is computed. Thus, the aramid favorably affected the energy consumption involved on the impact performance.

Figure 5 shows the Charpy samples after the test for both materials. The samples presented totally different fracture patterns; the CF/EP material was completely broken by the action of the hammer, while an important part of the CAF/EP sample remains uncut with clear evidence of delamination. The aramid reinforcement seems to have the sufficient resistance to failure necessary to deviate damage at the interlaminar region. This indicates that fragmentation of the CF/EP material, which failed in a more brittle manner

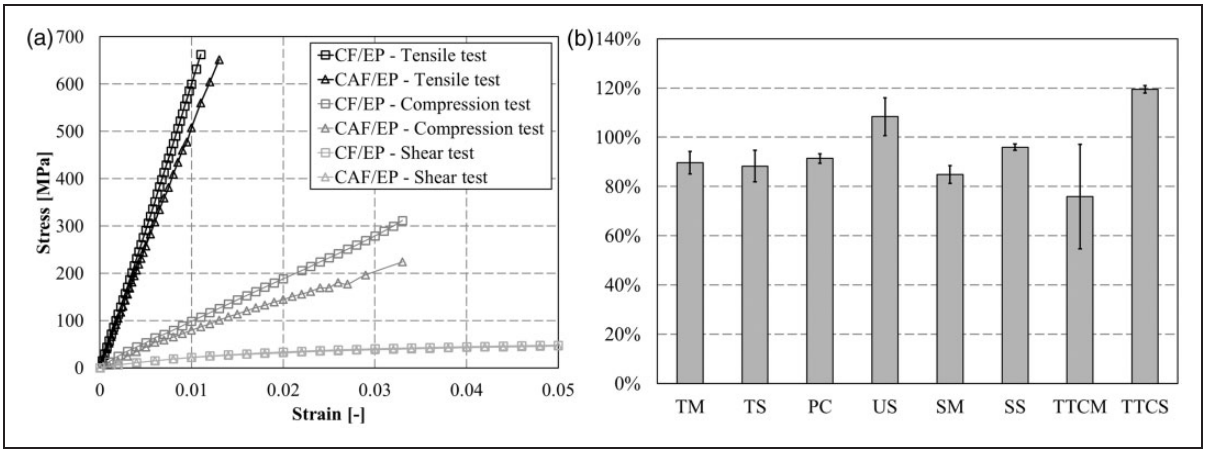

Figure 2. Representative stress-strain curves resulting from different tests (a) and the normalized mechanical properties for the CAF/EP composite (b). TM: tensile modulus; TS: tensile strength; PC: Poisson coefficient; US: ultimate strain; SM: shear modulus; SS: shear strength; TTCM: through thickness compression modulus; CS: compressive strength.

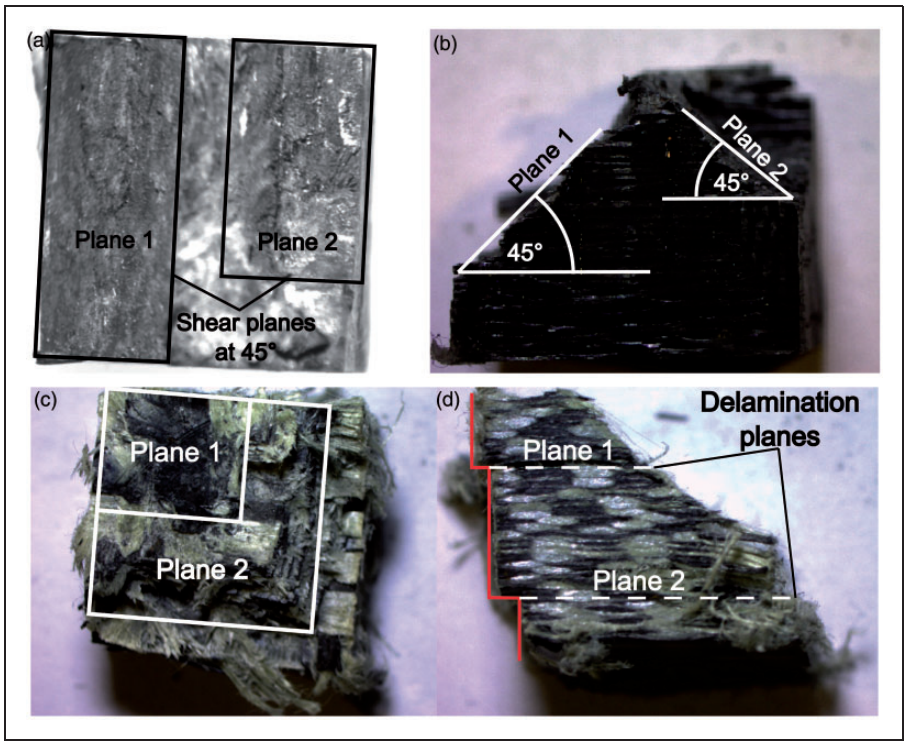

Figure 3. (a) top images and (b) lower images.

Table 3. Fracture properties.

Test	Parameter	Material	AV	SD	RSD	CI (95%)
Un-notched Charpy	Absorbed energy (J/m)	CF/EP	1673	218	13	±270
		CAF/EP	2307	280	12	±346
Fracture toughness	Initiation (MPa × $m^{0.5}$)	CF/EP	26.0	1.3	4.8	±1.8
		CAF/EP	29.3	1.5	5.0	±2.1
	Steady state (MPa × $m^{0.5}$)	CF/EP	31.4	2.4	7.7	±3.3
		CAF/EP	44.9	1.8	4.1	±2.5

Note: AV: average value; *SD*: standard deviation; RSD: relative standard deviation; CI: confidence interval; CF/EP: carbon/epoxy fiber; CAF/EP: carbon–aramid/epoxy fiber.

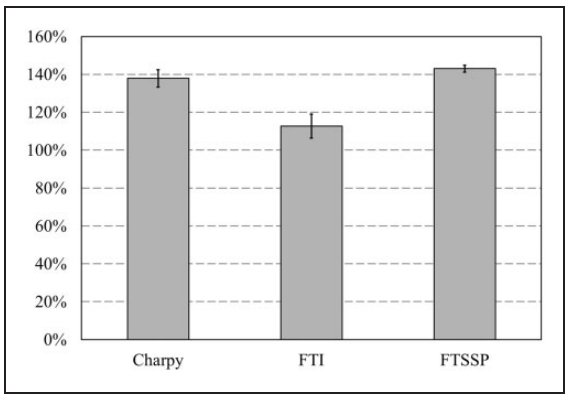

Figure 4. Normalized fracture properties for the CAF/EP composite. FTI: fracture toughness initiation; FTSSP: fracture toughness steady state propagation.

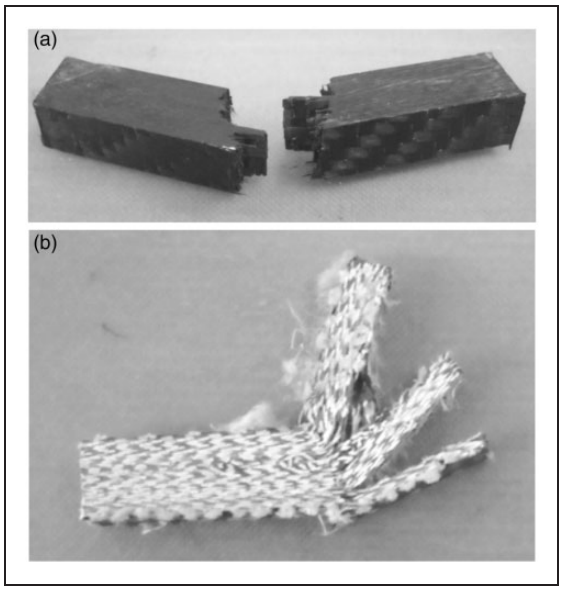

Figure 5. Fractured samples after Charpy test: CF/EP (a) and CAF/EP (b) composites.

involved less energy than the CAF/EP, where delamination promoted the deflection of the specimens consuming a higher level of energy. It is clear now that interlaminar failure, favored by the ductile behavior of aramid fibers, worked as an important toughening mechanism in CAF/EP specimens. The same hybrid effect has been observed by Dorigato and Pegoretti[36] where basalt hybridization of carbon/epoxy composites increased the energy absorption capacity of the samples due to an improvement of damage propagation resistance and delamination.

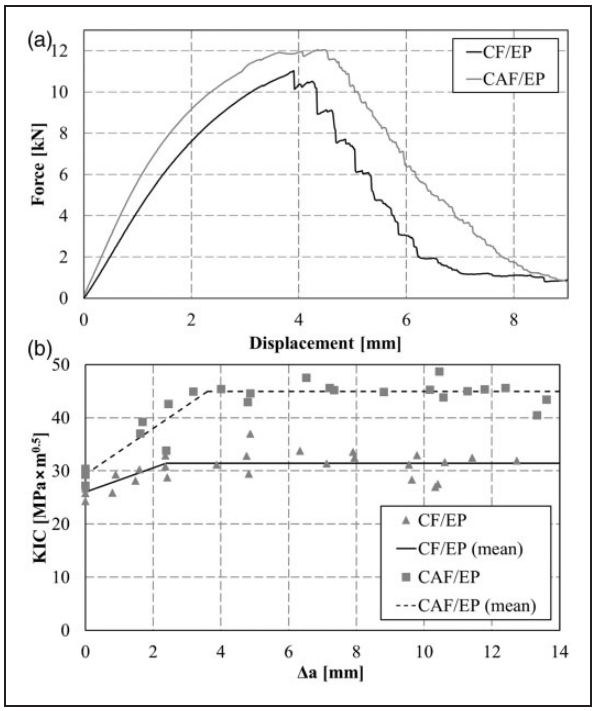

Figure 7. Representative force-displacement curves from the CT tests (a) and the resulting R-curves (b) for both composite materials.

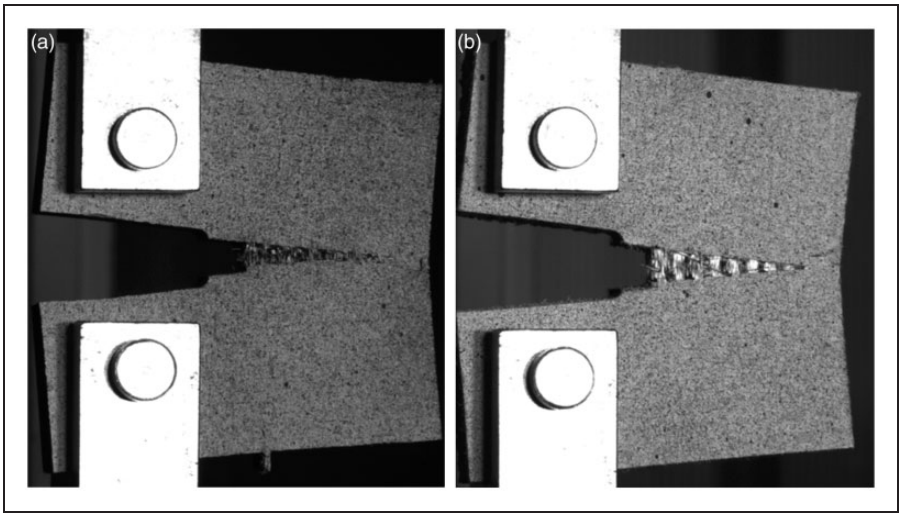

Figure 6. Fracture propagation in CF/EP (a) and CAF/EP (b) specimens at same displacement level on the CT test.

The CAF/EP configuration presented the highest values for both, initial fracture toughness and further propagation. The fracture toughness mode I test revealed increases of 12.6% on fracture initiation and 43% on the steady state propagation, as shown in Figure 4. As can be seen in Figure 6, some aramid fibers remained uncut even when the crack tip already moved away from their position in the measured surface and progressive failure is observed, which clearly enhanced the load-carrying capacity of the sample. This behavior was not exhibit by any of the CF/EP samples. Once again, the elongation capacity of the aramid fibers promoted a tougher response of the CAF/EP against fracture.

In Figure 7(a), the representative force–displacement curves from the CT tests for the CF/EP and CAF/EP composites are presented. Figure 7(b) shows the resulting crack growth resistance curves for both materials, where the positive influence of the aramid can be easily observed. Mean curves are plotted in order to facilitate the comparison. The CAF/EP composite presented a larger mean value of the crack extension (Δa) prior to reach the steady state propagation region, which defines the process cohesive zone.

Conclusions

This work assessed the influence of aramid fibers on the mechanical properties of hybrid aramid–carbon woven fabrics used as epoxy reinforcement under different mechanical conditions. The obtained results suggest that the improvements due to addition of aramid fibers are substantial in the case of energy absorption and fracture properties.

The experimental evidence revealed that despite a decrease of the overall stiffness and strength of the material, aramid fibers favorably affected the impact and fracture resistance of the composite. This is attributed to a more ductile response of aramid fiber compared to the carbon reinforcement.

This information is extremely useful in designing steps on high-performance applications, such as supports or pins for aircraft or aerospace structures, where the aramid behavior in fracture and impact properties can be greatly advantageous.

Funding

The author(s) disclosed receipt of the following financial support for the research, authorship, and/or publication of this article: The financial support by CONICYT through the projects Fondef D08i1138 and CONICYT Regional (CIPA/R08C1002) is gratefully acknowledged.

References

1. Friedrich K and Almajid AA. Manufacturing aspects of advanced polymer composites for automotive applications. *Appl Compos Mater* 2013; 20: 107–128.
2. Foster NG. Designing composite structures for optimum in-service performance with reference to the Firefly aircraft and the Jetstream baggage pod. *Proc IMechE, Part L: J Materials: Design and Applications* 2000; 214: 51–60.
3. Kretsis G. A review of the tensile, compressive, exural and shear properties of hybrid fibre-reinforced plastics. *Composites* 1987; 18: 13–23.
4. Ashby MF and Bréchet YJM. Designing hybrid materials. *Acta Mater* 2003; 51: 5801–5821.
5. Ashby MF. *Materials Selection in Mechanical Design*. 4th ed. Burlington: Butterworth-Heinemann, 2011.
6. Nunna S, Ravi Chandra P, Shrivastava S, et al. A review on mechanical behavior of natural fiber based hybrid composites. *J Reinf Plast Compos* 2012; 31: 759–769.
7. Gay D and Hoa SV. *Composite Materials. Design and Applications*. 2nd ed. Florida: CRC Press, 2007.
8. Nicolais L, Meo M and Milella E (eds). *Composite Materials. A Vision for the Future*. London: Springer, 2011.
9. Rahmani H, Mahmoudi SH and Ashori A. Mechanical performance of epoxy/carbon fiber laminated composites. *J Reinf Plast Compos* 2014; 33: 733–740.
10. CES Selector 2014 software. Granta Design Limited, Cambridge, UK, 2014, www.grantadesign.com
11. Hayashi T. Development of new material properties by hybrid composition (1st report). Fukugo Zairyo. *Compos Mater* 1972; 1: 18–20.
12. Phillips LN. The hybrid effect—does it exist? *Composites* 1976; 7: 7–8.
13. Zweben C. Tensile strength of hybrid composites. *J Mater Sci* 1977; 12: 1325–1337.
14. Fariborz SJ, Yang CL and Harlow DG. The tensile behavior of intraply hybrid composites I: model and simulation. *J Compos Mater* 1985; 19: 334–354.
15. Pandya KS, Veerraju C and Naik NK. Hybrid composites made of carbon and glass woven fabrics under quasi-static loading. *Mater Des* 2011; 32: 4094–4099.
16. Zhang J, Chaisombat K, He S, et al. Hybrid composite laminates reinforced with glass/carbon woven fabrics for lightweight load bearing structures. *Mater Des* 2012; 36: 75–80.
17. Banerjee S and Sankar B. Mechanical properties of hybrid composites using finite element method based micromechanics. *Compos Part B* 2014; 58: 318–327.
18. Li Y, Xian XJ, Choy CL, et al. Compressive and exural behavior of ultra-high-modulus polyethylene ber and carbon ber hybrid composites. *Compos Sci Technol* 1999; 59: 13–18.
19. Dong C and Davies IJ. Optimal design for the flexural behaviour of glass and carbon fibre reinforced polymer hybrid composites. *Mater Des* 2012; 37: 450–457.
20. Dong C and Davies IJ. Flexural properties of glass and carbon fiber reinforced epoxy hybrid composites. *J Materials: Design Appl* 2012; 227: 308–317.
21. Hosur MV, Adbullah M and Jeelani S. Studies on the low-velocity impact response of woven hybrid composites. *Compos Struct* 2005; 67: 253–262.
22. Valença SL, Griza S, de Oliveira VG, et al. Evaluation of the mechanical behavior of epoxy composite reinforced with Kevlar plain fabric and glass/Kevlar hybrid fabric. *Compos Part B* 2015; 70: 1–8.
23. Chiu CH, Tsai KH and Huang WJ. Crush-failure modes of 2D triaxially braided hybrid composite tubes. *Compos Sci Technol* 1999; 59: 1713–1723.

24. Kostar TD, Chou TW and Popper P. Characterization and comparative study of three-dimensional braided hybrid composites. *J Mater Sci* 2000; 35: 2175–2183.
25. Wan YZ, Chen GC, Huang Y, et al. Characterization of three-dimensional braided carbon/Kevlar hybrid composites for orthopedic usage. *Mater Sci Eng A Struct Mater* 2005; 398: 227–232.
26. Song JH. Pairing effect and tensile properties of laminated high-performance hybrid composites prepared using carbon/glass and carbon/aramid fibers. *Compos Part B* 2015; 79: 61–66.
27. Dorey G, Sidey GR and Hutchings J. Impact properties of carbon fibre/Kevlar 49 fibre hydrid composites. *Composites* 1978; 9: 25–32.
28. Marom G, Drukker E, Weinberg A, et al. Impact behaviour of carbon/Kevlar hybrid composites. *Composites* 1986; 17: 150–153.
29. Ma Y, Sugahara T, Yang Y, et al. A study on the energy absorption properties of carbon/aramid ber lament winding composite tube. *Compos Struct* 2015; 123: 301–311.
30. Kim BC, Park DC, Kim BJ, et al. Through-thickness compressive strength of a carbon/epoxy composite laminate. *Compos Struct* 2010; 92: 480–487.
31. Catalanotti G, Camanho PP, Xavier J, et al. Measurement of resistance curves in the longitudinal failure of composites using digital image correlation. *Compos Sci Technol* 2010; 70: 1986–1993.
32. Pinho ST, Robinson P and Iannucci L. Fracture toughness of the tensile and compressive fibre failure modes in laminated composites. *Compos Sci Technol* 2006; 66: 2069–2079.
33. Campbell FC. *Structural Composite Materials*. 1st ed. Ohio: ASM International, 2010.
34. Manders PW and Bader MG. The strength of hybrid glass/carbon fibre composites, Part 1 Failure strain enhancement and failure mode. *J Mater Sci* 1981; 16: 2233–2245.
35. González C and LLorca J. Mechanical behavior of unidirectional fiber-reinforced polymers under transverse compression: Microscopic mechanisms and modeling. *Compos Sci Technol* 2007; 67: 2795–2806.
36. Dorigato A and Pegoretti A. Flexural and impact behaviour of carbon/basalt fibers hybrid laminates. *J Compos Mater* 2014; 48: 1121–1130.